Applied Catalysis B: Environmental 336 (2023) 122914

Contents lists available at ScienceDirect

Applied Catalysis B: Environmental

journal homepage: www.elsevier.com/locate/apcatb

Cerium coordination-dependent surface intermediates regulate activity in dimethyl carbonate synthesis from CO_2 and methanol

Linyuan Tian [a,1], Zicong Tan [a,1], Quan Wang [a], Yin-Song Liao [b], Jyh-Pin Chou [c,*], Jyh-Ming Wu [b], Guoliang Liu [d,*], Yung-Kang Peng [a,e,**]

[a] Department of Chemistry, City University of Hong Kong, Hong Kong Special Administrative of China
[b] Department of Materials Science and Engineering, National Tsing Hua University, Hsinchu 300, Taiwan
[c] Department and Graduate Institute of Physics, National Changhua University of Education, Changhua 500, Taiwan
[d] College of Chemistry and Molecular Sciences, Wuhan University, Wuhan 430072, China
[e] City University of Hong Kong Shenzhen Research Institute, Shenzhen 518057, China

ARTICLE INFO

Keywords:
Dimethyl carbonate
CeO_2
Coordination structure
Surface methoxy species
Structure-activity relation

ABSTRACT

The direct synthesis of dimethyl carbonate (DMC) from CO_2 and methanol is a potential green alternative to the current industrial methods using toxic chemicals. Although many CeO_2-based catalysts have been explored, the key structural factor affecting their DMC activity is still unclear. Herein, single-crystalline CeO_2 catalysts bearing distinct but well-defined Ce coordination structures were examined. We found that methanol is the key species being activated by surface Ce sites (cf. CO_2) to produce methyl carbonate (MC) and later DMC. The reactivity of surface methoxy species towards CO_2 varies considerably with its configuration determined by Ce coordination structures. The head-to-head terminal methoxy species converts CO_2 to MC faster than its atilt counterparts, resulting in a higher DMC activity. The bridging methoxy species is, however, too stable to react with CO_2. The established structure-activity relation here should also guide the design of CeO_2-based catalysts in other reactions involving methanol activation.

1. Introduction

Dimethyl carbonate (DMC) is an important raw material in solvent [1–3], polymer synthesis [4], fuel/battery additives [5,6], etc. with a global market valued at US$ 467 million in 2016, expected to reach US$ 760 million by 2025 [7]. It is conventionally produced by methods that use explosive and toxic chemicals such as phosgene and carbon monoxide [8–10]. The direct synthesis of DMC by upgrading CO_2 with methanol has thus received much attention because of its environmentally benign nature [11,12]. In this reaction, CO_2 first reacts with methanol to form the intermediate species, methyl carbonate (MC), which is later converted to DMC in the presence of another methanol (see below).

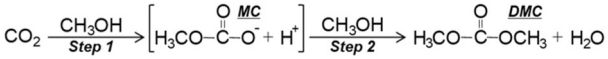

Over the past decade, the research interest in this green approach has mainly focused on developing CeO_2-based catalysts due to their decent activity among common oxide catalysts [12–21]. However, the key factor dictating their observed activity even for pristine CeO_2 is still unclear at present (Table 1). For example, early studies (entries 1–3) [13–15] showed that rod-shaped CeO_2 outperforms the other two shapes. They attributed this to various factors such as the amounts of acid/base sites (entry 1) [13], OH groups (entry 2) [14], and exposed (110) surface (entry 3) [15]. Based on the factor used, an opposite trend in DMC activity can be seen between the cube and octahedron (denoted as octa.) (e.g., cube > octa. in ref. [13] while octa. > cube in ref. [14, 15]). In fact, one can find in these reports that the activity of octa. (diameter > 300 nm) was unfairly compared to the rod (< 10 nm) and cube (< 50 nm) without considering the number of surface Ce sites (or at least surface area) involved in the reaction [13–15]. The preparation of their octa. using the phosphate as stabilizer (which chelates strongly to

* Corresponding authors.
** Corresponding author at: Department of Chemistry, City University of Hong Kong, Hong Kong Special Administrative of China.
E-mail addresses: jpchou@cc.ncue.edu.tw (J.-P. Chou), liugl@whu.edu.cn (G. Liu), ykpeng@cityu.edu.hk (Y.-K. Peng).
[1] These authors contributed equally to this work

https://doi.org/10.1016/j.apcatb.2023.122914
Received 20 March 2023; Received in revised form 21 May 2023; Accepted 23 May 2023
Available online 24 May 2023

Table 1
Activity comparison of CeO_2-based catalysts in the direct DMC synthesis.

Entry	Activity	NH_3/CO_2-TPD	Proposed Factor	Ref.
1	Rod > Cube > Octa.	Yes	acid-basic sites	[13]
2	Rod > Octa. > Cube	No	-OH groups	[14]
3	Rod > Octa. > Cube	No	(110) surface	[15]
4	$Zr_{0.1}Ce_{0.9}O_2$ rod > CeO_2 rod	Yes	oxygen vacancy-related acid-basic sites	[16]
5	$Ti_{0.04}Ce_{0.96}O_2$ rod > CeO_2 rod	Yes	acid-basic sites with medium strength	[17]
6	Fe-doped CeO_2 rod > CeO_2 rod	Yes	acid-basic sites with medium strength	[18]
7	CeO_2 rod > Co/Ni/Ca/ Cu-doped CeO_2 rod	Yes	no correlation with either strength or concentration of acid-basic sites	[19]
8	CeO_2 > La/Gd/Pr-doped CeO_2 (particle)	Yes	a balanced acidity/basicity ratio	[20]
9	CeO_2 > Zr/Ni/Cu/Zn-doped CeO_2 (particle)	Yes	a balanced acidity/basicity ratio	[21]

surface Ce sites [22,23]) may also hinder the adsorption and subsequent activation of reactants, resulting in low activity.

Despite the apparent flaws in early reports, recent studies mainly focus on rod-shaped CeO_2 and its surface engineering for catalytic improvement (entries 4–7) [16–19]. Liu et al. attributed a 30% increase in DMC activity of $Zr_{0.1}Ce_{0.9}O_2$ rods (cf. pristine CeO_2 rods) to its higher concentration of oxygen vacancy (V_o)-related acid-basic sites (entry 4) [16]. A similar increase in activity was also observed for $Ti_{0.04}Ce_{0.96}O_2$ rods[17] (entry 5) and Fe-doped CeO_2 rods[18] (entry 6), while they attributed this to the enhanced number of acid-basic sites with medium strength. Interestingly, the doping of hetero atoms was also reported to impose an opposite effect on DMC activity (entries 7–9) [19–21]. Al-Darwish et al. showed that the yield of DMC decreases a lot after doping CeO_2 rods with Co/Ni/Ca/Cu, and no correlation can be found for the strength/ concentration of their acid-basic sites (entry 7) [19]. Stoian et al. [20] and Giram et al. [21] observed a decrease in DMC activity for La/Gd/Pr-doped (entry 8) and Zr/Ni/Cu/Zn-doped (entry 9) CeO_2 particles, while they attributed this to the imbalanced acidity/basicity ratio. In our opinion, different interpretation (even disagreement) found above on the doping effect on surface acid/base properties and DMC activities could be due to the heavy reliance on the use of NH_3/CO_2 temperature programmed desorption (TPD) for acidity/basicity characterization (e.g., entry 1 and entries 4–9) [24]. The simple correlations between catalytic activity and overall properties like acidity/basicity (also for V_o and OH groups) maybe useful in a practical sense but they do not necessarily help to identify active sites and the corresponding catalytic mechanism [25–27]. The "coordination structure" of active sites is convoluted in a way that affects the acidity/basicity revealed by NH_3/CO_2-TPD in these reports. First of all, the use of NH_3 as TPD probe for CeO_2 surfaces may not reflect the adsorption of methanol (not even for its activation) due to the difference in their geometric nature. Secondly, oxygen becomes labile on CeO_2 surfaces at elevated temperature (especially > 250 °C) [28–31]. The change of Ce/O coordination structures and hence the obtained acidity/basicity in TPD (up to 800 °C) may deviate significantly from their actual one for this reaction at 140 °C. The doping of foreign atoms to CeO_2 surfaces (entries 4–9) further complicates the coordination structure of Ce/O sites, making it even more difficult to approach the true structure-activity relation for this reaction.

As is known, heterogeneous catalysis is closely associated with not only the adsorption of reactants but their later activation at catalytically active sites on solids' surface. Given this, "coordination structure" engineering of Ce/O sites on pristine CeO_2 surfaces is believed to regulate the activation of adsorbed methanol/CO_2 and hence DMC production. Scheme 1 displays the bulk CeO_2 in fluorite structure and the atomic arrangements of three low-index surfaces.[28–30] Due to the suspension of crystal growth, Ce atom exposed on pristine (111) surface is 7-coordinated with a missing oxygen atop (denoted as $Ce_{7c(111)}$, Scheme 1a). This leaves a vacant orbital perpendicular to the surface, which is expected to form an adduct bond with the lone pair electron(s) of the coming reactant [25,32]. Although Ce atoms hosted by pristine (110) (denoted as $Ce_{6c(110)}$, Scheme 1b) and (100) (denoted as $Ce_{6c(100)}$, Scheme 1c) surfaces are both 6-coordinated with two missing oxygens, the geometry of the resulting vacant orbitals is different due to the crystallographic orientation of their host. These surface Ce sites enclosed by various coordination structures in terms of (i) coordination number and (ii) local geometry are believed to interact very differently with a given reactant. This, together with their high structural uniformity, allows an in-depth and precise mechanistic study of the adsorption/ activation of methanol/CO_2 in the title reaction. Note that these coordination unsaturated Ce sites on crystal surfaces are distinct from typical V_o-associated Ce sites bearing poor structural uniformity often discussed in the literature [28–30]. This point has been comprehensively reviewed in our recent reports [31,32].

To establish a reliable structure-activity relation for these Ce sites in direct DMC synthesis, experiments should be ideally done on well-

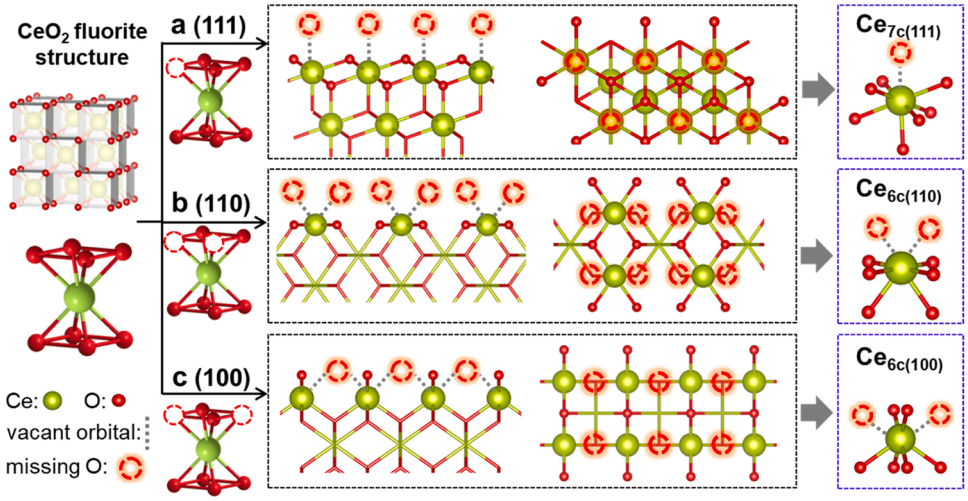

Scheme 1. Crystallographic structures for pristine CeO2 (a) (111), (b) (110), and (c) (100) surfaces and the coordination structures for corresponding surface $Ce_{7c(111)}$, $Ce_{6c(110)}$, and $Ce_{6c(100)}$ sites. Note that the surface model of (100) with half of the surface oxygen removed was adopted in this study since this configuration was concluded the most probable one and has been widely used for catalytic correlation in the literature [28–30].

defined CeO_2 surfaces such as single crystals to ensure the obtained results are interpretable and scientifically meaningful. Given the difficulty in obtaining single crystal surfaces with high surface area, single-crystalline CeO_2 nanoparticles (NPs) of octahedron, rod, and cube shapes enclosed preferentially by (111), (110), and (100) surface were adopted in this study. Both experimental and theoretical results suggest that methanol is the key reactant being activated (cf. CO_2) for the production of MC and later DMC. The dissociative adsorption of this molecule on pristine CeO_2 surfaces gives surface methoxy species in various configurations depending on the coordination structure of Ce sites. Most importantly, these surface methoxy species were found to display various reactivity towards CO_2 and MC, resulting in extreme DMC activity.

2. Experimental section

2.1. Catalyst preparation

CeO_2 shapes were synthesized according to our previous report [32]. Briefly, CeO_2 cube and rod were hydrothermally synthesized using cerium nitrate hexahydrate as cerium source and NaOH solution for pH control. For CeO_2 cube, 0.651 g of $Ce(NO_3)_3$•6 H_2O and 3.6 g of NaOH were mixed in 30 mL H_2O and stirred for 30 min under room temperature. The mixture for CeO_2 rod was prepared similarly but the amount of NaOH was doubled to 7.2 g. The mixture was then heated in Teflon-lined stainless steel under 180 °C (for CeO_2 cube) and 100 °C (for CeO_2 rod) for 24 h. CeO_2 octa. was prepared by mixing 0.8141 g of Ce $(NO_3)_3$•6 H_2O and 0.7005 g of hexamethylenetetramine (HMT) in 110 mL H_2O for 3 h at 75 °C. All products were washed with ethanol for 5 times and then dried in the oven at 60 °C overnight. To remove HMT, the CeO_2 octa. was calcined under air at 200 °C for 12 h. For a fair comparison, CeO_2 cube and rod were also calcinated under the same condition before use.

2.2. Catalytic testing

The dimethyl carbonate synthesis from CO_2 and methanol was conducted in an autoclave. In a typical testing, the autoclave containing 15 mL methanol and 50 mg catalyst was firstly purged with CO_2 for 4–5 times to remove air and then filled with 4 MPa CO_2 before heating up to 413 K for 3 h. After reaction, 1-hexanol (0.1 mL) was added to the solution as an internal standard substance for a quantitative analysis. All products were analyzed by GC-MS (Agilent 5890, column-HP5, 30 m × 0.25 mm × 0.25 μm) and GC (Agilent 6890, column-TG-5SilMS, 30 m × 0.25 mm × 0.25 μm). The concentration of DMC in solution was determined by integrating the areas of the peaks of DMC and 1-hexanol, and then the resulting value was compared with internal standards. The turnover frequency (TON) of DMC was calculated by equation: $TON_{product} = N_{product}/(N_{Ce\ sites\ on\ surface})$. For the calculation of activation energy, their initial rate was obtained at 393, 413, 433, 453 K by sampling at 30 and 60 min

2.3. Material characterization

X-ray diffraction (XRD, D2 PHASER 2nd gen, Bruker) with monochromatized Cu Kα radiation was used to identify the crystalline phases of CeO_2. Transmission electron microscope (TEM, Philips Technai 12) spectral was employed to investigate the morphology for CeO_2 samples. High-resolution Transmission electron microscope (HRTEM, JEOL 1200 F) with an acceleration voltage of 200 kV was used to identify their corresponding lattice spacings. DRTFTS (Diffuse Reflectance Fourier-Transform Spectroscopy) spectra were acquired on a VERTEX 70 (Bruker). For catalysts used in DRIFT experiments below were all pretreated in IR cell with argon flow (40 mL/min) at 140 ℃ for 30 min to clean the surface. (1) The introduction of one reactant to CeO_2 shapes pre-adsorbed with the other reactant. The adsorption of 1st reactant (methanol or CO_2): methanol (carried by argon)/CO_2 was introduced into IR cell (40 mL/min) for 30 min at 140 ℃. The introduction of 2nd reactant: argon flow was first purged (40 mL/min) for 5 min to remove non-adsorbed methanol/CO_2 followed by the introduction of the other reactant as elaborated above. (2) Temperature-programmed desorption (TPD) of adsorbed methanol from CeO_2 shapes. The adsorption of methanol (carried by argon) was conducted at 30 °C for 30 min followed by heating up to 140 °C (10 °C/min) in argon (40 mL/min) and held for 5 min at 60, 100, 120, and 140 °C before spectrum recording. For CO_2/NH_3-TPD, all catalysts (50 mg) were first pretreated at 150 °C for 1 h under He. Their adsorption was conducted at 30 °C for 1 h under CO_2 (15 vol% of CO_2 in He, 40 mL/min) or NH_3 (15 vol% of NH_3 in He, 40 mL/min) flow carried by N_2 (15 vol% CO_2/NH_3, 40 mL/min). The samples were purged with He (40 mL/min) to remove physically adsorbed CO_2 or NH_3. Subsequently, samples were heated under the constant He flow (40 mL/min) and, at the same time, TPD signals were recorded from 50 to 800 °C at a ramp rate of 10 °C/min.

2.4. Density functional theory (DFT) calculation

The density functional theoretical calculations were performed in plane-wave based software, Vienna ab-initio Simulation Package (VASP) [33]. The electron-ion interaction is described by the projected augmented wave (PAW) [34] method with cut-off energy of 680 eV. The exchange-correlation effects are treated in the scheme of Perdew–Burke–Ernzerhof (PBE) [35] in generalized gradient approximation. The Brillouin zone of primitive cell was sampling within the *k*-mesh of 4 × 4 × 4. All the structural relaxation are performed under the criterion of 10^{-5} eV for the electronic self-consistent loop. Moreover, with a view to obtaining accurate results, the DFT + *U* method introduced by Dudarev [36] was considered with a value of 3.125 eV [37] for on-site Coulomb interactions of cerium atom. The surface polarity of (100) surface was cancelled by removing half of the surface oxygen from the fully oxygen coverage, making it cation to anion in stoichiometry [38]. The six-layered 2 × 2 surface models of (100), (110), and (111) with vacuum thickness larger than 20Å are constructed for the adsorption calculations [38]. During the calculations, except for the bottom trilayer are fixed, the rest atoms are allowed to relax. The adsorption energy (E_{ads}) is obtained through the equation:

$$E_{ads} = E_{total} - E_{surface} - E_{adsorbates}$$

where the, E_{total}, $E_{surface}$, and $E_{adsorbates}$ represent the total energy of the adsorption system, the pristine surfaces, and the adsorbates (methanol and CO_2 molecules). To investigate the kinetic properties of reactions, the climbing image nudged-elastic band method (CI-NEB) with the force-based optimizer, fast inertial relaxation engine (FIRE) [39], is implemented to study the reaction path for distinguished molecules synthesis on three different surfaces [40,41]. In this part, the surface models are extended to a 4 × 4 supercell in order to avoid the interactions among periodic reactant images.

3. Results and discussion

3.1. CeO_2 preparation and catalytic testing

CeO_2 nanocrystallites in the shape of octa (Fig. 1a), rod (Fig. 1b), and cube (Fig. 1c) with comparable sizes were synthesized according to our previous report.[31] The high-resolution TEM image of CeO_2 octa. confirms its (111) termination with a lattice spacing of 0.32 nm. For CeO_2 rod, lattices paralleled to the surface can be identified with a spacing of 0.19 nm, suggesting the preferential exposure of (110) surface for this shape. The cube sample mainly exposes (100) surface as evidenced by the lattice spacing of 0.27 nm. Their morphology and fluorite structure were further verified by scanning transmission electron microscope (STEM) (Fig. S1), powder X-ray diffraction (PXRD) (Fig. S2), and the Fast Fourier transform patterns embedded in Fig. 1. Although TEM/

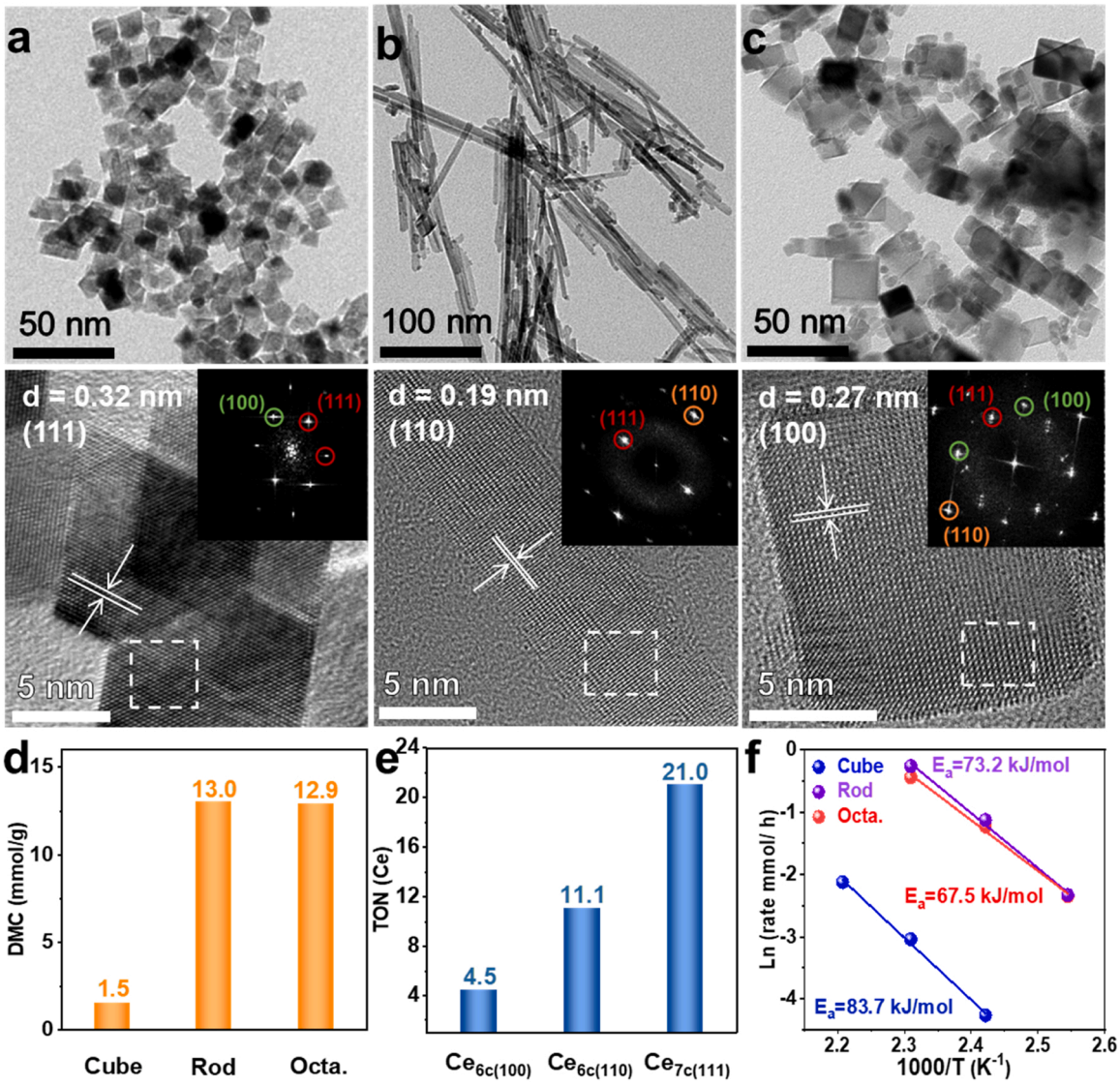

Fig. 1. Transmission electron microscope (TEM) images of CeO_2 (a) octa., (b) rod, (c) cube, and their corresponding high-resolution TEM images and Fast Fourier transform patterns (row below). (d) Activity and (e) turnover number (TON) for CeO_2 shapes in DMC synthesis and (f) the Arrhenius plots for their activation energy.

STEM used above cannot reveal the actual distribution of facets for each shape, our recent study using probe-assisted NMR [42–45] showed that ≥ 90% surface of octa., rod, and cube prepared by our method is enclosed by (111), (110), and (100) surface (see SI for details, Fig. S3) [31]. The position and width of their NMR signals suggest that the hosted $Ce_{7c(111)}$, $Ce_{6c(110)}$, and $Ce_{6c(100)}$ sites are well-separated with comparable site uniformity (from the full width at half maximum (FWHM)), which is essential to approach a reliable structure-activity relation for the title reaction.

Direct DMC synthesis from methanol and CO_2 was then tested on CeO_2 shapes (see the experimental section for details). As shown in Fig. 1d, octa. and rod produce a similar amount of DMC, which is much higher than that of the cube with methanol conversion of 0.35%, 0.36%, and 0.04%, respectively, in 3 h. Note that methanol is not only the reactant but also the solvent used in this reaction. This, together with the equilibrium methanol conversion of 0.7% in the absence of dehydrant [46], explains the low methanol conversion obtained here and in the reports [16,17,20,46]. Their morphology (Fig. S4) and fluorite structure (Fig. S5) were both kept after the reaction. Since the surface area and terminal surface are both different among samples (Table 2), turnover number (TON) was further calculated for discussion. Here, the TON is defined as the number of moles of DMC produced per mole of surface Ce sites during the reaction period. Given ≥ 90% facet purity for each shape, we only consider their dominant surface here to simplify the discussion below. The concentration of surface Ce sites (mmol/g) for CeO_2 shapes (Table 2) was approached by their surface area (m^2/g) and the number of Ce sites per nm^2 of the dominant surface (see Fig. S6 for the calculation of this value for each surface). As displayed in Fig. 1e, the TON of $Ce_{7c(111)}$ is nearly doubled and five times higher than that of $Ce_{6c(110)}$ and $Ce_{6c(100)}$, respectively, matching the trend in activation energy of their host shape (Fig. 1f) (i.e., octa. < rod < cube (Table S1), also see Table S2 for the comparison with CeO_2 samples in the literature). Although a slight decrease in TON can be seen for all Ce sites in the

Table 2
Comparison of factors among CeO_2 shapes.

Sample	Surface	# of Ce per nm^2	BET (m^2/g)	Ce density (mmol/g)	TON	XPS ratio	
						Ce^{3+}/Ce^{4+}	O_s/O_L
Cube	(100)	6.86	29	0.33	4.5	0.39	0.49
Rod	(110)	4.85	144	1.16	11.1	0.43	0.47
Octa.	(111)	7.92	46	0.61	21.0	0.39	0.45

second and third rounds (Fig. S7), $Ce_{7c(111)}$ is still the most active site followed by $Ce_{6c(110)}$ and $Ce_{6c(100)}$ with a maintained difference in their activity.

3.2. Discussion on factors proposed in the literature

To evaluate the role of overall physicochemical properties such as V_o, OH group, and acid-basic sites often suggested in the literature (Table 1), CeO_2 shapes were further characterized by electron paramagnetic resonance (EPR), X-ray photoelectron spectroscopy (XPS), and NH_3/CO_2-TPD. The EPR signal at approximately $g = 2.00$ is often assigned to the unpaired electrons trapped in surface V_o by adsorbed O_2 [47]. Given no such signal being observed for all CeO_2 shapes at room temperature and 77 K (Fig. S8), the contribution of surface V_o-associated Ce sites to the activity is thus negligible compared to that of abundant surface coordination unsaturated Ce sites on crystal surface (Scheme 1). This result can also be evidenced by the similar Ce^{3+}/Ce^{4+} ratio (Table 2) obtained from their XPS Ce_{3d} spectra (Fig. S9). The quantity of surface OH groups was approached from the corresponding XPS O_{1s} range. As shown in Figure S10, all shapes exhibit a main peak of lattice oxygens (O_L) at 529.6 eV and a shoulder peak of surface O-relevant species (O_S) at 531.5 eV with a similar O_S/O_L ratio (Table 2). This, together with the negligible V_o revealed by EPR, suggests that CeO_2 shapes bear a comparable amount of surface OH groups, which again cannot account for their extreme activity (Fig. 1d-f). NH_3/CO_2-TPD was also employed to study their surface acid/base properties. In general, desorption peaks for both molecules with temperature < 200 °C, 200–400 °C, and > 400 °C correspond to weak, medium, and strong acid/basic sites, respectively [13, 16–21]. Surprisingly, a similar NH_3-TPD pattern with desorption peaks at about 300 °C and 440 °C was obtained for octa. and cube (Fig. S11a), suggesting the presence of medium and strong acid sites on them. Although the octa. bears a higher amount of acid sites at these two strengths (cf. the cube), this doesn't explain why the TON of $Ce_{7c(111)}$ is ca. 5 times higher than that of $Ce_{6c(100)}$ (Fig. 1e) with a much lower activation energy (Fig. 1f). One may attribute this to the co-presence of moderate basic sites on octa. (cf. cube at about 275 °C) revealed by CO_2-TPD (Fig. S11b). However, the rod bearing this kind of basic site with higher concentration only provides comparable activity per mass (cf. octa, Fig. 1d). Therefore, we found it difficult to establish a solid correlation for CeO_2 shapes based on their NH_3/CO_2-TPD results in this study. One should also bear in mind that the coordination structure of Ce sites varies with temperature especially at > 250 °C [28–31]. This makes the correlation of NH_3/CO_2-TPD results to the title reaction often tested at ca. 140 °C in doubt. Taking all into account, these overall physicochemical properties revealed by conventional surface tools are far from satisfactory [24] and hence result in different interpretations in the literature (Table 1).

3.3. Identifying the key factor and reactant

Based on the discussion above, the extreme activity observed for CeO_2 shapes (Fig. 1d-f) should thus be closely associated with their abundant Ce sites enclosed by various coordination structures (Scheme 1). Given this, the question lies on the adsorption/activation of which reactant (methanol or CO_2) by these surface Ce sites accounts for the observed activity (or TON). We first examined their adsorption by density functional theory (DFT) calculation since a given reactant is unlikely to be activated without adsorption in this reaction. As shown in Fig. 2a, CO_2 adsorbs weakly on all pristine CeO_2 surfaces with adsorption energy ($|E_{ad}|$) smaller than 0.2 eV (0.05 eV for $Ce_{7c(111)}$; 0.11 eV for $Ce_{6c(110)}$; 0.17 eV for $Ce_{6c(100)}$). Since the thermal energy at 140 °C is ca. 0.04 eV, CO_2 could thus barely adsorb on the most active $Ce_{7c(111)}$ here and hence should plays a negligible role in the reaction condition. To confirm this, the desorption of CO_2 on the octa. at elevated temperature was evaluated by DRIFTS (diffuse reflectance infrared Fourier transform spectroscopy) [the sample was pre-cleaned at 140 ℃ under argon for 30 mins followed by CO_2 adsorption at 60 °C for another 30 mins]. As shown in Fig. S12, the intensity of the IR signals of surface adsorbed CO_2 species (e.g., carbonate species at 1620 cm^{-1}) decreases sharply at elevated temperature and can be barely seen at 140 ℃. Since $Ce_{7c(111)}$ displays the highest DMC activity (Fig. 1e), this result suggests that the adsorption of CO_2 (also for its later activation) should play a negligible role in affecting the observed DMC activity. In contrast, DFT calculation suggests that methanol adsorbs much stronger on all pristine CeO_2 surfaces with higher $|E_{ad}|$ (> 0.4 eV, Fig. 2b). Note that the dissociative adsorption of methanol was considered for these surface Ce sites here since the barrier for the formation of methoxy and OH groups on (111) and (110) surfaces is very small (no barrier was found for (100) surface, Fig. S13). The undissociated form bearing low Lewis basicity is also unlikely to react with CO_2. [13,16,46] As is expected, the configuration of methoxy species is closely associated with the coordination structure of surface Ce sites (Scheme 1). The O atom of methoxy tends to bind head-to-head to $Ce_{7c(111)}$ via its vertical vacant orbital, giving the $|E_{ad}|$ of 0.48 eV (Fig. 2b(i)). A higher $|E_{ad}|$ was obtained when this O atom forms a chemical bond with $Ce_{6c(110)}$ along the direction of one of the vacant orbitals (1.14 eV, Fig. 2b(ii)). Given the distinct local structure, the methoxy O atom is shared by two $Ce_{6c(100)}$ sites in a bridging form, resulting in the highest $|E_{ad}|$ of 1.67 eV. Although the angle of the as-formed Ce-O bonds slightly deviates from their rigid model due to the surface relaxation, this result suggests that the coordination structure of Ce sites could play a key role in affecting the configuration of surface methoxy species (and their reactivity, vide infra).

We then conducted DRIFTS for methanol pre-adsorbed CeO_2 shapes to confirm the configuration of these methoxy species and their physicochemical properties at elevated temperature [the sample was pre-cleaned at 140 ℃ under argon for 30 mins followed by methanol adsorption at 60 °C for another 30 mins]. As shown in Fig. 3, all shapes

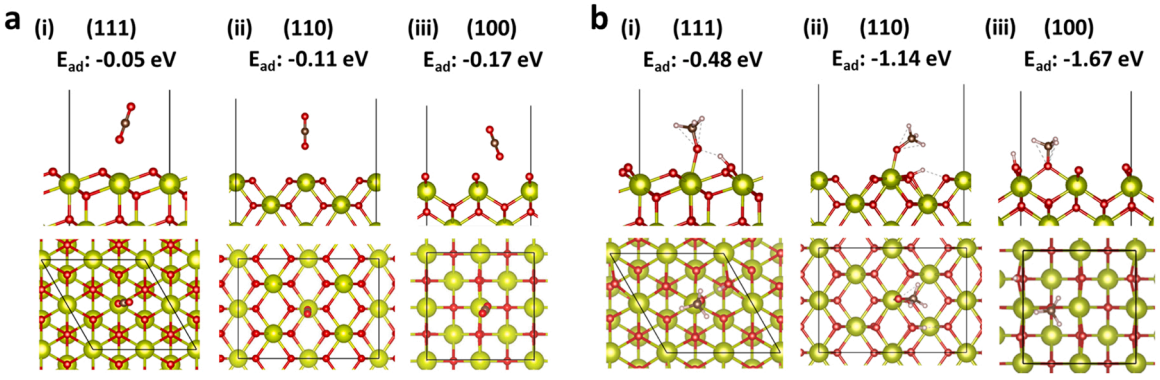

Fig. 2. The calculated adsorption energy (E_{ad}) and configuration of (a) CO_2 and (b) methanol on pristine CeO_2 (i) (111), (ii) (110), and (iii) (100) surfaces.

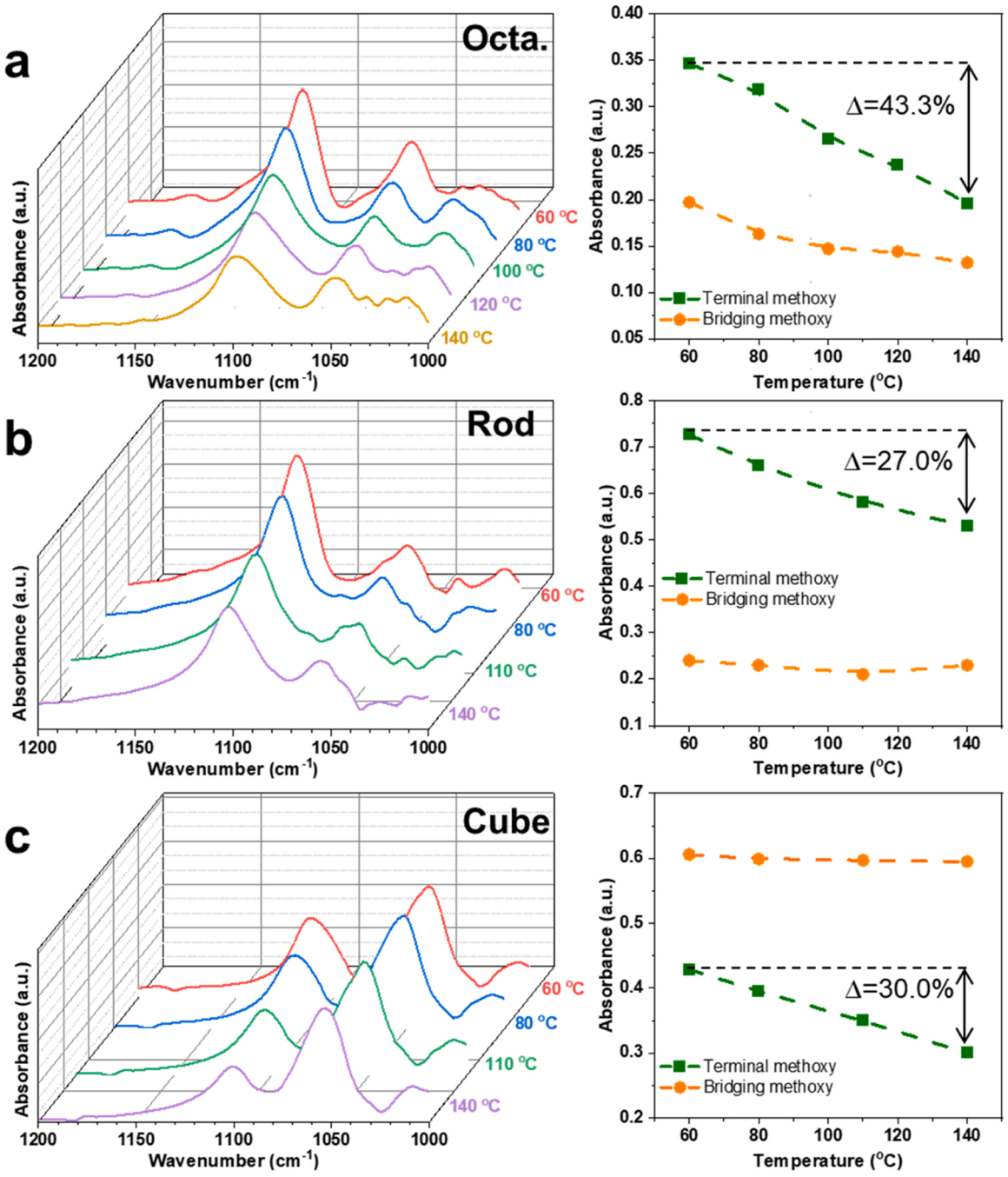

Fig. 3. The desorption of surface terminal (~1100 cm^{-1}) and bridging (~1050 cm^{-1}) methoxy species at elevated temperature on (a) octahedron, (b) rod, and (c) cube revealed by DRIFTS.

reveal two IR bands at around 1100 cm^{-1} and 1050 cm^{-1} upon methanol adsorption. The signal at a higher frequency is often attributed to the terminal methoxy group and the one with a lower frequency comes from the bridging methoxy group [48,49]. The majority of the surface methoxy species are found in the terminal form on octa. (Fig. 3a)/rod (Fig. 3b) and bridging form on cube (Fig. 3c), matching well with the DFT results of their dominant surface. The minor IR signal observed for each sample can be attributed to the presence of minor surface or defective sites on the major surface as revealed by their ^{31}P NMR signals (Fig. S3). Although terminal methoxy species formed on $Ce_{7c(111)}$ (head-to-head, Fig. 2b(i)) and $Ce_{6c(110)}$ (atilt, Fig. 2b(ii)) are not distinguishable by their IR frequency at 1100 cm^{-1} between octa. and rod samples, the difference in their E_{ad} should affect their population remained on the sample at elevated temperature.[48,49] Indeed, the terminal methoxy species formed on octa. was found to desorb more easily (Fig. 3a) than its counterpart on rod (Fig. 3b) at elevated temperature. While only a minor loss of the bridging methoxy species can be seen for both samples due to its high stability. A similar trend can also be seen for terminal/bridging methoxy species on the cube (Fig. 3c). This result confirms that the configuration and physicochemical properties of surface methoxy species differ with Ce coordination structures and should hence affect their reactivity towards CO_2 and MC in direct DMC production.

3.4. Surface methoxy species-mediated MC and DMC production

DRIFTS was further adopted to study the reactivity of these methoxy species towards CO_2 at 140 °C. The CeO_2 sample was pre-cleaned at 140 ℃ under argon for 30 mins followed by methanol adsorption at 140 °C for another 30 mins before passing CO_2 (Fig. 4a). Upon the introduction of CO_2, the evolving of IR signals at 1600, 1464, 1347, and 1196 cm^{-1} (dot highlighted) suggests the formation of surface MC species (step 1) (Table S3) [15,16,50], which can later be converted to the product, DMC, with another surface methoxy species (step 2). Interestingly, the fate of MC species varies a lot among CeO_2 samples. For example, MC signals reach the maximum in 1 min on methanol pre-adsorbed octa., followed by a gradual decrease with time (Fig. 4a (i)). The formation of DMC is thus the rate-limiting step as previously suggested in the literature [46]. Since the IR signal of bridging methoxy species at 1050 cm^{-1} is nearly unchanged in the presence of CO_2 (Fig. S14), the head-to-head terminal methoxy species formed on $Ce_{7c(111)}$ (at 1100 cm^{-1}) is thus suggested to be the key species [48,49] being converted to MC and DMC in both steps. For the methanol pre-adsorbed rod, IR pattern of MC saturates in ca. 5 min (Fig. 4a(ii)), implying that the atilt methoxy species produced on $Ce_{6c(110)}$ is less reactive to CO_2 due to its higher stability (Fig. 2b(ii)). This sample then displays a slow decrease of MC signals (i.e., DMC production) with a rate comparable to that of octa. (Fig. 4a(ii)) as also evidenced by their comparable activation energy (Fig. 1f). The formation of MC on the methanol pre-adsorbed cube is further suppressed without saturation after passing CO_2 for 30 min (Fig. 4a(iii)), suggesting that the bridging methoxy species formed on $Ce_{6c(100)}$ is very stable (with the highest $|E_{ad}|$, Fig. 2b(iii)) and hence nearly inert in both steps. We perceive that the tiny amount of DMC produced by the cube may be attributed to the presence of $Ce_{6c(110)}$ sites on its minor (110) surface (~10%, see ^{31}P NMR spectrum in Fig. S3). The emerging of IR signals at ca. 1420 and 1335 cm^{-1} observed for this sample upon CO_2 induction could be attributed to the formation of surface bicarbonate [51] and formate-like [48] species, respectively.

As a control DRIFTS experiment, CO_2 was pre-adsorbed on CeO_2 shapes at 140 ℃ before passing methanol (Fig. 4b) [the sample was pre-cleaned at 140 ℃ under argon for 30 mins followed by CO_2 adsorption at 140 °C for another 30 mins before introducing methanol]. The formation of carbonate species with a dominant IR band at ca. 1620 cm^{-1} were identified on all CeO_2 samples, which could be attributed to the adsorption of CO_2 on their defective Ce sites [51]. Although this signal decreases considerably after passing methanol and disappears in the end, no production of MC was observed even for the octa. We reason that this is due to the removal of these weakly adsorbed CO_2 species by the coming methanol as evidenced by the emerging of surface methoxy species on the octa. after passing methanol for 1 min at 140 ℃ (Fig. S15). This result confirms again that CO_2 is not the key molecule being activated for the production of MC and later DMC. Instead, methanol plays a crucial role in both steps with reactivity closely associated with its adsorbed configuration, which is determined by the coordination structure of Ce sites. To further confirm this, we fed methanol and CO_2 at the same time to CeO_2 samples and monitored the IR pattern

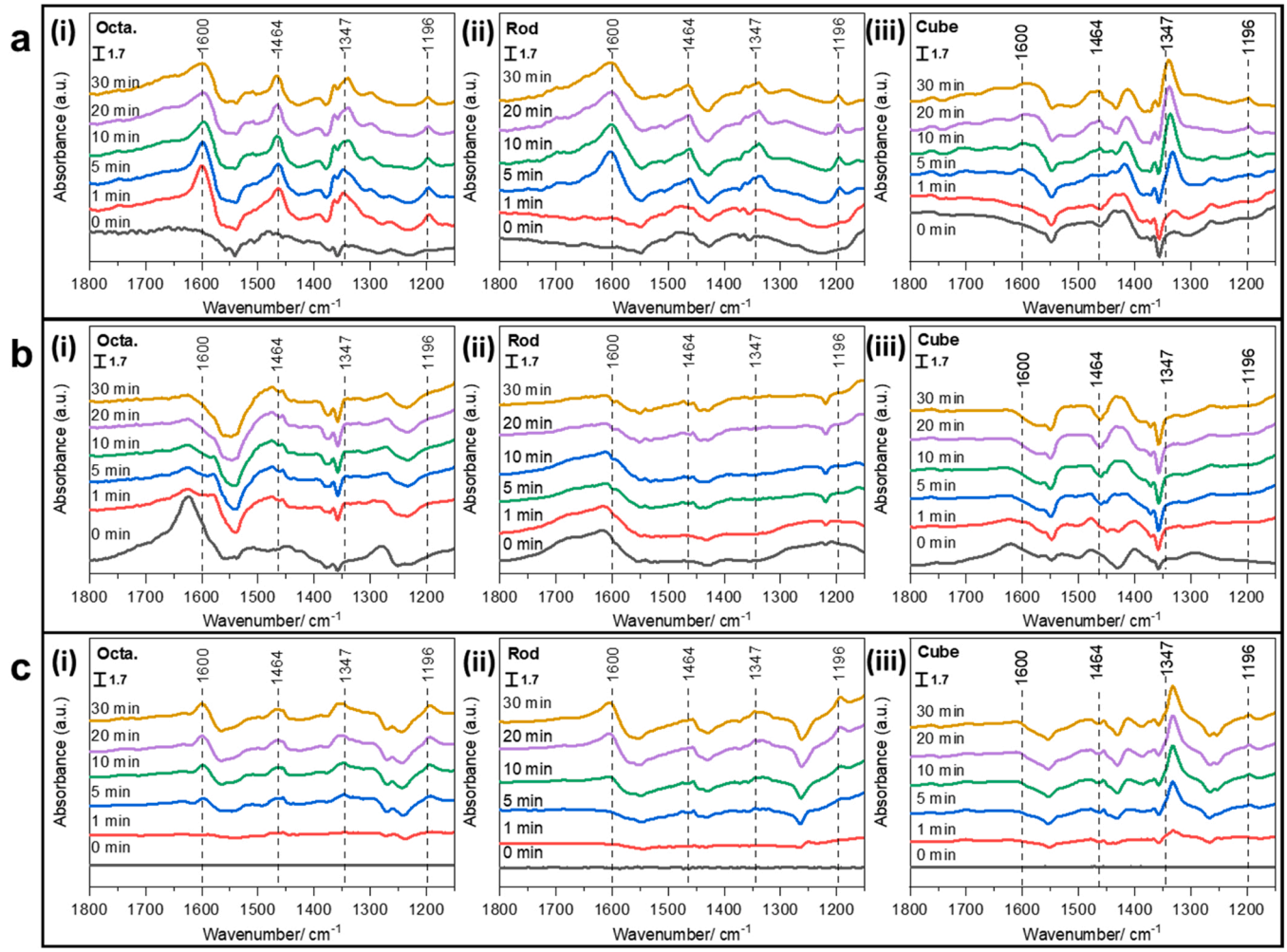

Fig. 4. DRIFTS spectra for CeO_2 (i) octa., (ii) rod, and (iii) cube (a) pre-adsorbed with methanol followed by passing CO_2 at 140 ℃, (b) pre-adsorbed with CO_2 followed by passing methanol at 140 ℃, and (c) passing both methanol and CO_2 at 140 ℃.

of MC with time [the sample was pre-cleaned at 140 ℃ under argon for 30 mins before passing both methanol and CO_2] (Fig. 4c). As expected, MC emerges again on CeO_2 samples with IR signals evolving slower than their methanol pre-adsorbed case in Fig. 4a.

3.5. DFT study on the reaction mechanism

To support the structure-activity observed above, the formation of MC (Fig. 5a) and its later conversion to DMC (Fig. 5b,c) on pristine CeO_2 surfaces were further investigated by the climbing image nudged-elastic band method (CI-NEB) calculations. As shown in Fig. 5a (see details in Figs. S16-S18), CO_2 first approaches surface methoxy species (the initial structure, IS) followed by the nucleophilic attack of its C atom (C_{CO2}) by methoxy O ($O_{methoxy}$) (the intermediate, IM). This step bents CO_2 from its linear structure and promotes the formation of new bond(s) between O_{CO2} and another surface Ce. Eventually, MC species (the final structure, FS) can be produced on CeO_2 surface by breaking the $O_{methoxy}$-Ce bond (s). As expected, surface methoxy species in various configurations show distinct reactivity towards CO_2 in this step. The insertion of CO_2 into terminal methoxy species requires only 0.22 eV for its head-to-head form on (111) surface (Fig. 5a(i)) while 1.06 eV is needed for its atilt form on (110) surface (Fig. 5a(ii)). An even higher activation energy of 1.34 eV is required for the bridged methoxy species on (100) surface to conduct this step (Fig. 5a(iii)). The size of this barrier is believed to be closely associated with their stability (or adsorption energy, Fig. 2b) and the distance between Ce sites on these surfaces. Most importantly, the trend in barrier size (i.e., (100) > (110) > (111)) can well explain the rate of MC generation in step 1 observed for CeO_2 shapes (octa. > rod > cube) in DRIFT experiments (Fig. 4a). The configuration of the resulting MC species was also found in terminal form on (111)/(110) surface and bridging form on (100) surface (Fig. 5a) as that of methoxy species (Fig. 2b). Although the MC species is less atilt here on (110) surface due to its bulkier group, further decrease of the angle of the as-formed Ce-O bond on this surface (from ca. 84–75 degrees) was only found to slightly enhance the energy by 60 meV. This result suggests that the methoxy (or MC) species can tilt in a range of degrees on (110) surface with a relatively flat potential energy surface.

To further produce DMC, two pathways have been suggested in the literature [46,50,52] for the reaction between MC and another methoxy species as follows (Fig. 5b): (i) nucleophilic addition of methoxy species to MC species and (ii) electrophilic addition of methyl species to MC species. For the pathway (i), we found that the distances between nearby methoxy and MC species on CeO_2 surfaces are too far for the oxygen of the former species to nucleophilically attack the carbonyl group of the latter species. This, together with the steric hindrance imposed by the -OCH_3 group of MC species, suggested a significant energy barrier across all CeO_2 surfaces and hence unlikely the key pathway contributing to their observed activity. For the (ii) electrophilic addition pathway, the reaction barrier was calculated to be 1.10 eV for both (111) (Fig. 5c(i)) and (110) (Fig. 5c(ii)) surfaces (see details in Fig. S19 and Fig. S20), which explains their comparable activation energy obtained in Fig. 1f. In comparison, the bridging methoxy species and bridging MC species produced on (100) surface were both found to be too stable to form DMC via this pathway. This result further supports our previous assumption that the tiny amount of DMC observed on the cube could be attributed to the presence of $Ce_{6c(110)}$ sites on its minor (110) surface (~10%, Fig. S3).

Scheme 2 summarizes the structure-activity relation for these Ce sites in the title reaction based on the above experimental and theoretical results. The head-to-head terminal methoxy species produced on $Ce_{7c(111)}$ converts CO_2 to terminal MC species at a rate faster than its atilt counterparts found on $Ce_{6c(110)}$. While the subsequent methylation of the as-formed terminal MC species on both Ce sites by another terminal methoxy species is much slower. The poor activity of $Ce_{6c(100)}$ can be attributed to the formation of bridging methoxy species, which is too

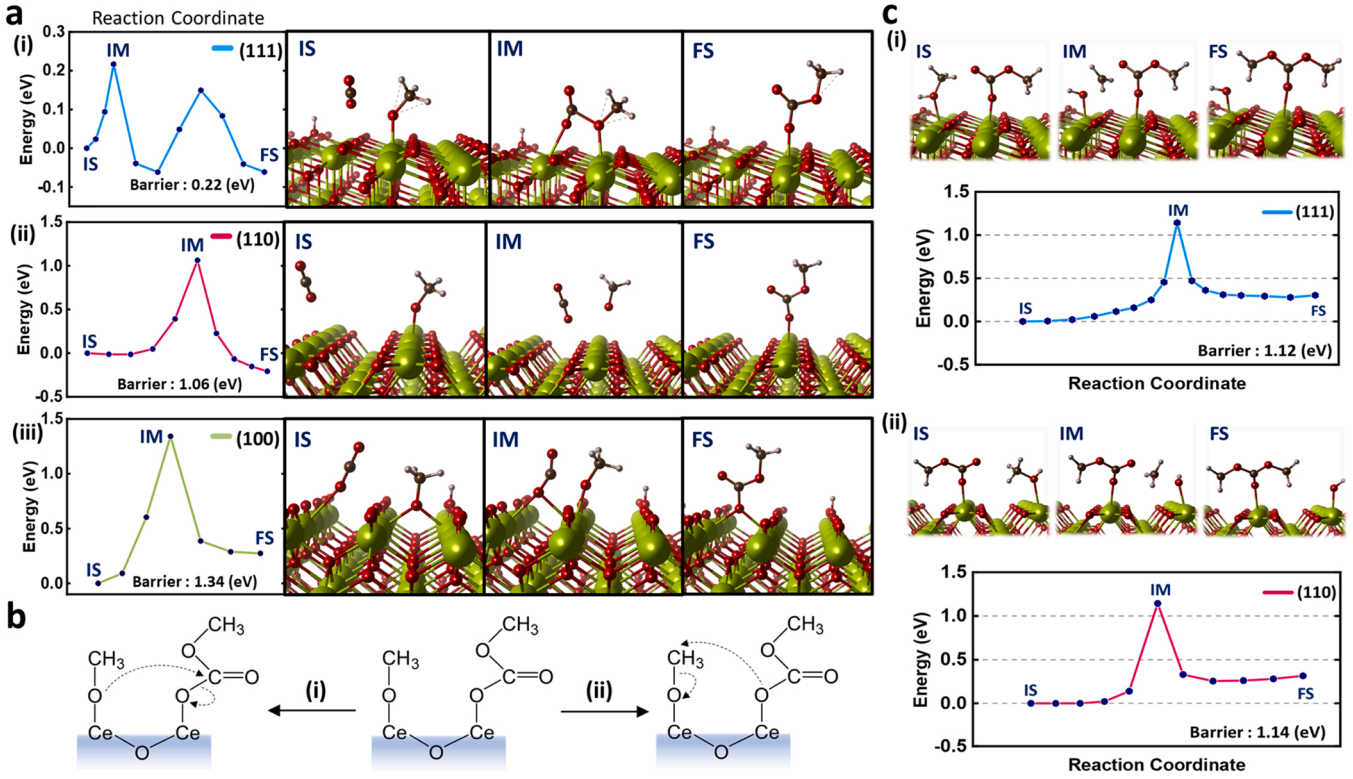

Fig. 5. (a) The energy profiles for the formation of MC on CeO_2 (i) (111), (ii) (110), and (iii) (100) surfaces. The IS, IM, and FS indicate the initial structure, intermediate structure, and final structure, respectively. The cerium, oxygen, carbon, and hydrogen atoms are represented in green, red, brown, and pink, respectively. (b) Schematic illustration of DMC formation by (i) nucleophilic addition of methoxy species and (ii) electrophilic addition of methyl species to surface MC species. (c) The energy profiles for the formation of DMC on CeO_2 (i) (111) and (ii) (110) surfaces.

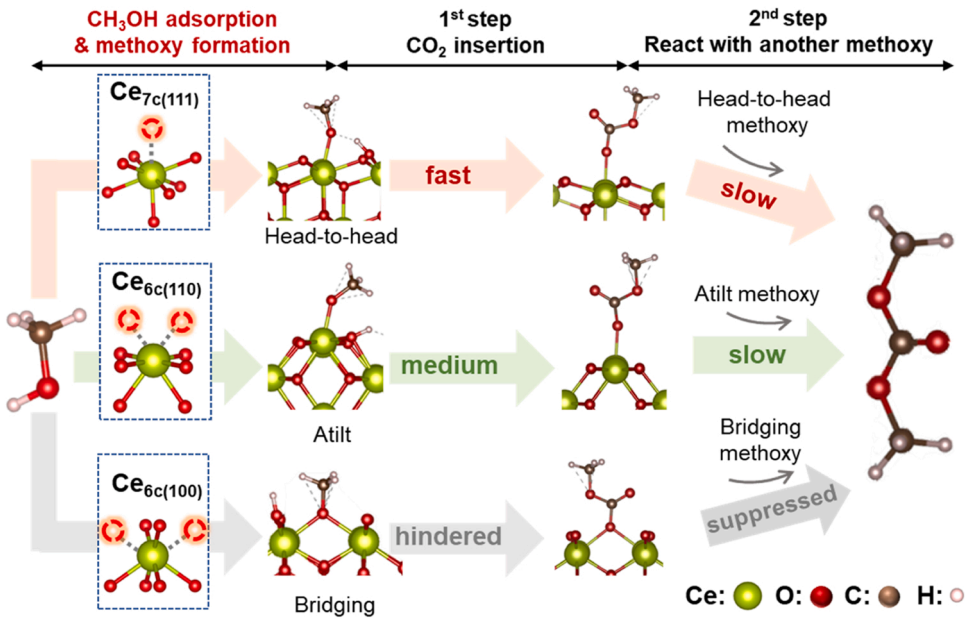

Scheme 2. The proposed structure-activity relation for Ce sites bearing various coordination structures in the direct DMC synthesis.

stable to catalyze both steps in this reaction.

4. Conclusions

In this study, $Ce_{7c(111)}$, $Ce_{6c(110)}$, and $Ce_{6c(100)}$ sites bearing various coordination structures were used to establish their structure-activity relation in direct DMC synthesis from CO_2 and methanol. These Ce sites were hosted by CeO_2 crystallites of well-defined octa., rod, and cube shapes, respectively, to ensure their coordination structure is uniform enough for interpretable and meaningful data. The calculated TON shows that the DMC activity is in the order of $Ce_{7c(111)} > Ce_{6c(110)} > Ce_{6c(100)}$, matching well with the trend of activation energy obtained for their host shape. Both DFT and DRIFT results suggest that methanol is the key species being activated by surface Ce sites to produce MC and later DMC. During the reaction, methanol first undergoes dissociative adsorption on Ce sites, forming surface methoxy species with its configuration (and reactivity) determined by Ce coordination structures. The head-to-head terminal methoxy species on $Ce_{7c(111)}$ was found to produce terminal MC species with CO_2 at a rate faster than its atilt counterparts on $Ce_{6c(110)}$. The subsequent methylation of the as-formed terminal MC species by another terminal methoxy species is much slower on both Ce sites (cf. their rate for step 1), hence the rate-limiting step of this reaction. As for $Ce_{6c(100)}$, the bridging methoxy species barely produces MC species with CO_2 due to its high stability. Since bridging methoxy/MC species are too stable to form DMC, the observed activity of the cube was attributed to the tiny amount of $Ce_{6c(110)}$ sites on its minor (110) surface. This work thus highlights that one can simply regulate the reactivity (or configuration) of the adsorbed reactants by tuning the coordination structure of the active sites on a pristine material. The structure-activity relation established in this work is expected to guide the design and synthesis of CeO_2-based catalysts in not only this reaction but also other reactions such as methanol decomposition, methanolysis, and methoxylation involving methanol activation.

CRediT authorship contribution statement

Linyuan Tian: Investigation, Formal analysis, Writing – original draft. **Zicong Tan**: Investigation, Formal analysis, Writing – original draft. **Quan Wang**: Methodology. **Yin-Song Liao**: Methodology. **Jyh-Pin Chou**: Investigation, Resources. **Jyh-Ming Wu**: Investigation, Resources. **Guoliang Liu**: Investigation, Resources. **Yung-Kang Peng**: Conceptualization, Writing – original draft, Writing – review & editing, Supervision, Funding acquisition.

Declaration of Competing Interest

The authors declare the following financial interests/personal relationships which may be considered as potential competing interests: Yung Kang Peng reports financial support was provided by Hong Kong Research Grants Council. Yung Kang Peng reports financial support was provided by Strategic Interdisciplinary Research Grant of City University of Hong Kong. Yung Kang Peng reports financial support from the MOST (Taiwan) and National Center for High-performance Computing of National Applied Research Laboratories (NARLabs) in Taiwan.

Data Availability

Data will be made available on request.

Acknowledgements

We thank the Hong Kong Research Grants Council (CityU 21301719 and 11300020) and the Strategic Interdisciplinary Research Grant of City University of Hong Kong (Project No. 7020053). J.C. Chou acknowledges financial support from the MOST, Taiwan (MOST-109-2112-M-018-008-MY3) and National Center for High-performance Computing (NCHC) of National Applied Research Laboratories (NARLabs) in Taiwan for providing computational and storage resources.

Appendix A. Supporting information

Supplementary data associated with this article can be found in the online version at doi:10.1016/j.apcatb.2023.122914.

References

[1] M. Tudorache, A. Negoi, B. Tudora, V.I. Parvulescu, Environmental-friendly strategy for biocatalytic conversion of waste glycerol to glycerol carbonate, Appl. Catal., B 146 (2014) 274–278.
[2] F.S.H. Simanjuntak, J.S. Choi, G. Lee, H.J. Lee, S.D. Lee, M. Cheong, H.S. Kim, H. Lee, Synthesis of glycerol carbonate from the transesterification of dimethyl carbonate with glycerol using DABCO and DABCO-anchored Merrifield resin, Appl. Catal., B 165 (2015) 642–650.

[3] S. Zhang, Z. Xia, Y. Zou, F. Cao, Y. Liu, Y. Ma, Y. Qu, Interfacial frustrated Lewis pairs of CeO_2 activate CO_2 for selective tandem transformation of olefins and CO_2 into cyclic carbonates, J. Am. Chem. Soc. 141 (2019) 11353–11357.

[4] K. Tomishige, Y. Gu, Y. Nakagawa, M. Tamura, Reaction of CO_2 with alcohols to linear-, cyclic-, and poly-carbonates using CeO_2-based catalysts, Front. Energy Res. 8 (2020) 117.

[5] P. Kumar, P. With, V.C. Srivastava, R. Gläser, I.M. Mishra, Efficient ceria-zirconium oxide catalyst for carbon dioxide conversions: characterization, catalytic activity and thermodynamic study, J. Alloy. Compd. 696 (2017) 718–726.

[6] B. Zhang, G. Ding, H. Zheng, Y. Zhu, Transesterification of dimethyl carbonate with tetrahydrofurfuryl alcohol on the K_2CO_3/ZrO_2 catalyst-Function of the surface carboxylate species, Appl. Catal., B 152 (2014) 226–232.

[7] Global Dimethyl Carbonate Market 2017–2025, https://www.businesswire.com/news/home/20180212005686/en/Global-Dimethyl-Carbonate-Market-2017–2025—Market.

[8] M.A. Pacheco, C.L. Marshall, Review of dimethyl carbonate (DMC) manufacture and its characteristics as a fuel additive, Energy Fuels 11 (1997) 2–29.

[9] M. Richter, M. Fait, R. Eckelt, E. Schreier, M. Schneider, M.-M. Pohl, R. Fricke, Oxidative gas phase carbonylation of methanol to dimethyl carbonate over chloride-free Cu-impregnated zeolite Y catalysts at elevated pressure, Appl. Catal., B 73 (2007) 269–281.

[10] S. Ji, Y. Chen, G. Zhao, Y. Wang, W. Sun, Z. Zhang, Y. Lu, D. Wang, Atomic-level insights into the steric hindrance effect of single-atom Pd catalyst to boost the synthesis of dimethyl carbonate, Appl. Catal., B 304 (2022), 120922.

[11] D. Shi, S. Heyte, M. Capron, S. Paul, Catalytic processes for the direct synthesis of dimethyl carbonate from CO_2 and methanol: a review, Green. Chem. 24 (2022) 1067–1089.

[12] K. Tomishige, Y. Gu, T. Chang, M. Tamura, Y. Nakagawa, Catalytic function of CeO_2 in non-reductive conversion of CO_2 with alcohols, Mater. Today Sustain. 9 (2020), 100035.

[13] S. Wang, L. Zhao, W. Wang, Y. Zhao, G. Zhang, X. Ma, J. Gong, Morphology control of ceria nanocrystals for catalytic conversion of CO_2 with methanol, Nanoscale 5 (2013) 5582–5588.

[14] S.P. Wang, J.J. Zhou, S.Y. Zhao, Y.J. Zhao, X.B. Ma, Enhancements of dimethyl carbonate synthesis from methanol and carbon dioxide: The in situ hydrolysis of 2-cyanopyridine and crystal face effect of ceria, Chin. Chem. Lett. 26 (2015) 1096–1100.

[15] S.Y. Zhao, S.P. Wang, Y.J. Zhao, X.B. Ma, An in situ infrared study of dimethyl carbonate synthesis from carbon dioxide and methanol over well-shaped CeO_2, Chin. Chem. Lett. 28 (2017) 65–69.

[16] B. Liu, C. Li, G. Zhang, X. Yao, S.S.C. Chuang, Z. Li, Oxygen vacancy promoting dimethyl carbonate synthesis from CO_2 and methanol over Zr-doped CeO_2 nanorods, ACS Catal. 8 (2018) 10446–10456.

[17] Z. Fu, Y. Zhong, Y. Yu, L. Long, M. Xiao, D. Han, S. Wang, Y. Meng, TiO_2-doped CeO_2 nanorod catalyst for direct conversion of CO_2 and CH_3OH to dimethyl carbonate: catalytic performance and kinetic study, ACS Omega 3 (2018) 198–207.

[18] M. Luo, T. Qin, Q. Liu, Z. Yang, F. Wang, H. Li, Novel Fe-modified CeO_2 nanorod catalyst for the dimethyl carbonate formation from CO_2 and methanol, ChemCatChem (2022).

[19] J. Al-Darwish, M. Senter, S. Lawson, F. Rezaei, A.A. Rownaghi, Ceria nanostructured catalysts for conversion of methanol and carbon dioxide to dimethyl carbonate, Catal. Today 350 (2020) 120–126.

[20] D. Stoian, F. Medina, A. Urakawa, Improving the stability of CeO_2 catalyst by rare earth metal promotion and molecular insights in the dimethyl carbonate synthesis from CO_2 and methanol with 2-cyanopyridine, ACS Catal. 8 (2018) 3181–3193.

[21] G.G. Giram, V.V. Bokade, S. Darbha, Direct synthesis of diethyl carbonate from ethanol and carbon dioxide over ceria catalysts, N. J. Chem. 42 (2018) 17546–17552.

[22] T. Yao, Z. Tian, Y. Zhang, Y. Qu, Phosphatase-like activity of porous nanorods of CeO_2 for the highly stabilized dephosphorylation under interferences, ACS Appl. Mater. Interfaces 11 (2018) 195–201.

[23] Z. Tan, T.S. Wu, Y.L. Soo, Y.K. Peng, Unravelling the true active site for CeO_2-catalyzed dephosphorylation, Appl. Catal., B 264 (2020), 118508.

[24] Y.K. Peng, S.E. Tsang, Facet-dependent photocatalysis of nanosize semiconductive metal oxides and progress of their characterization, Nano Today 18 (2018) 15–34.

[25] X. Ma, H. Xin, Orbitalwise coordination number for predicting adsorption properties of metal nanocatalysts, Phys. Rev. Lett. 118 (2017), 036101.

[26] R. Qin, K. Liu, Q. Wu, N. Zheng, Surface coordination chemistry of atomically dispersed metal catalysts, Chem. Rev. 120 (2020) 11810–11899.

[27] C. Vogt, B.M. Weckhuysen, The concept of active site in heterogeneous catalysis, Nat. Rev. Chem. 6 (2022) 89–111.

[28] T. Montini, M. Melchionna, M. Monai, P. Fornasiero, Fundamentals and catalytic applications of CeO_2-based materials, Chem. Rev. 116 (2016) 5987–6041.

[29] A. Trovarelli, J. Llorca, Ceria catalysts at nanoscale: how do crystal shapes shape catalysis? ACS Catal. 7 (2017) 4716–4735.

[30] Y. Ma, W. Gao, Z. Zhang, S. Zhang, Z. Tian, Y. Liu, J.C. Ho, Y. Qu, Regulating the surface of nanoceria and its applications in heterogeneous catalysis, Surf. Sci. Rep. 73 (2018) 1–36.

[31] Z. Tan, G. Li, H.L. Chou, Y. Li, X. Yi, A.H. Mahadi, A. Zheng, S.C. Edman Tsang, Y. K. Peng, Differentiating surface Ce Species among CeO_2 facets by solid-state NMR for catalytic correlation, ACS Catal. 10 (2020) 4003–4011.

[32] Z. Tan, J. Zhang, Y.C. Chen, J.P. Chou, Y.K. Peng, Unravelling the role of structural geometry and chemical state of well-defined oxygen vacancies on pristine CeO_2 for H_2O_2 activation, J. Phys. Chem. Lett. 11 (2020) 5390–5396.

[33] G. Kresse, J. Furthmüller, Efficient iterative schemes for ab initio total-energy calculations using a plane-wave basis set, Phys. Rev. B 54 (1996) 11169.

[34] G. Kresse, D. Joubert, From ultrasoft pseudopotentials to the projector augmented-wave method, Phys. Rev. B 59 (1999) 1758.

[35] J.P. Perdew, K. Burke, M. Ernzerhof, Generalized gradient approximation made simple, Phys. Rev. Lett. 77 (1996) 3865.

[36] S.L. Dudarev, G.A. Botton, S.Y. Savrasov, C. Humphreys, A.P. Sutton, Electron-energy-loss spectra and the structural stability of nickel oxide: an LSDA+ U study, Phys. Rev. B 57 (1998) 1505.

[37] C. Loschen, J. Carrasco, K.M. Neyman, F. Illas, First-principles LDA+ U and GGA+ U study of cerium oxides: Dependence on the effective U parameter, Phys. Rev. B 75 (2007), 035115.

[38] M. Nolan, S. Grigoleit, D.C. Sayle, S.C. Parker, G.W. Watson, Density functional theory studies of the structure and electronic structure of pure and defective low index surfaces of ceria, Surf. Sci. 576 (2005) 217–229.

[39] E. Bitzek, P. Koskinen, F. Gähler, M. Moseler, P. Gumbsch, Structural relaxation made simple, Phys. Rev. Lett. 97 (2006), 170201.

[40] G. Henkelman, H. Jónsson, Improved tangent estimate in the nudged elastic band method for finding minimum energy paths and saddle points, J. Chem. Phys. 113 (2000) 9978–9985.

[41] G. Henkelman, B.P. Uberuaga, H. Jónsson, A climbing image nudged elastic band method for finding saddle points and minimum energy paths, J. Chem. Phys. 113 (2000) 9901–9904.

[42] Y.K. Peng, H.L. Chou, S.C. Edman Tsang, Differentiating surface titanium chemical states of anatase TiO_2 functionalized with various groups, Chem. Sci. 9 (2018) 2493–2500.

[43] Y.K. Peng, B. Keeling, Y. Li, J. Zheng, T. Chen, H.L. Chou, T.J. Puchtler, R. A. Taylor, S.C.E. Tsang, Unravelling the key role of surface features behind facet-dependent photocatalysis of anatase TiO_2, Chem. Commun. 55 (2019) 4415–4418.

[44] Q. Wang, X. Yi, Y.C. Chen, Y. Xiao, A. Zheng, J.L. Chen, Y.K. Peng, Electronic state manipulation of surface titanium activates dephosphorylation over TiO_2 near room temperature, Angew. Chem., Int. Ed. Engl. 133 (2021) 16285–16291.

[45] G. Sun, M.M.J. Li, K. Nakagawa, G. Li, T.S. Wu, Y.K. Peng, Bulk-to-nano regulation of layered metal oxide gears H_2O_2 activation pathway for its stoichiometric utilization in selective oxidation reaction, Appl. Catal. B 313 (2022), 121461.

[46] M. Honda, M. Tamura, Y. Nakagawa, K. Nakao, K. Suzuki, K. Tomishige, Organic carbonate synthesis from CO_2 and alcohol over CeO_2 with 2-cyanopyridine: scope and mechanistic studies, J. Catal. 318 (2014) 95–107.

[47] Y.K. Peng, Y. Fu, L. Zhang, I.F. Teixeira, L. Ye, H. He, S.C.E. Tsang, Probe-molecule-assisted NMR spectroscopy: a comparison with photoluminescence and electron paramagnetic resonance spectroscopy as a characterization tool in facet-specific photocatalysis, ChemCatChem 9 (2017) 155–160.

[48] Z. Wu, M. Li, D.R. Mullins, S.H. Overbury, Probing the surface sites of CeO_2 nanocrystals with well-defined surface planes via methanol adsorption and desorption, ACS Catal. 2 (2012) 2224–2234.

[49] Z. Qi, L. Chen, S. Zhang, J. Su, G.A. Somorjai, Mechanism of methanol decomposition over single-site Pt_1/CeO_2 catalyst: a DRIFTS study, J. Am. Chem. Soc. 143 (2020) 60–64.

[50] Y. Yoshida, Y. Arai, S. Kado, K. Kunimori, K. Tomishige, Direct synthesis of organic carbonates from the reaction of CO_2 with methanol and ethanol over CeO_2 catalysts, Catal. Today 115 (2006) 95–101.

[51] Z.J. Gong, Y.R. Li, H.L. Wu, S.D. Lin, W.-Y. Yu, Direct copolymerization of carbon dioxide and 1, 4-butanediol enhanced by ceria nanorod catalyst, Appl. Catal. B 265 (2020), 118524.

[52] R. Juárez, P. Concepción, A. Corma, H. García, Ceria nanoparticles as heterogeneous catalyst for CO_2 fixation by ω-aminoalcohols, Chem. Commun. 46 (2010) 4181–4183.